Establishing correlations among pore structure, surface roughness, compressive strength, and fracture toughness of ceramic water filters local to Rajasthan, India

Amrita Kaurwar Nighojkar[a], Ashish Kumar Agrawal[b], Balwant Singh[c], Sandeep Gupta[a], Raj Kumar Satankar[a], Jerry Mathew Oommen[a], Lovelesh Dave[a], Muhammad Sharif[d], A.B.O Soboyejo[e], Anand Plappally[a,*]

[a]*Mechanical Engineering Department, Indian Institute of Technology Jodhpur, Jodhpur, Rajasthan 342037, India,*
emails: anandk@iitj.ac.in (A. Plappally), kaurwar.1@iitj.ac.in (A.K. Nighojkar), gupta.5@iitj.ac.in (S. Gupta),
pg201383005@iitj.ac.in (R.K. Satankar), oommen.1@iitj.ac.in (J.M. Oommen), ldave@iitj.ac.in (L. Dave)
[b]*Imaging Beamline (BL-4), Indus-2, Raja Ramanna Centre for Advanced Technology, Indore 452013, India,*
email: ashishka@rrcat.gov.in
[c]*Indus-2, Raja Ramanna Centre for Advanced Technology, Indore 452013, India, email: balwants@rrcat.gov.in*
[d]*Aerospace Engineering and Mechanics Department, University of Alabama, Tuscaloosa, AL 35487, USA,*
email: msharif@eng.us.edu
[e]*Food, Agriculture and Biological Engineering, Ohio State University, Columbus, OH 43210, USA, email: soboyejo.2@osu.edu*

ABSTRACT

This article discusses the characterization of local clay-organic (CO) ceramics used in the microfiltration application in India. Local clay and sawdust were the raw materials for these ceramics. Wet mix with specified volume fractions of these raw materials was hydroplastically formed to square plates, cured, and fired at 850°C. Once fired, these ceramics showed a prominent presence of silica, alumina, and oxides of iron. Quartz, potassium feldspar, and hematite are the major minerals in these ceramics. The dominance of pores orthogonal to the surface was a feature in this family of ceramics. The 50O composition of the CO ceramics is observed to have a maximum frequency of orthogonal pores. Therefore, an example of gravity-based filtration flow models of this material shaped in distinct forms is carried out to enumerate possible scaling. The surface roughness of the cured specimen plate varies linearly with the porosity of the mixture. The compressive strength shows a polynomial increase with an increase in the values of surface roughness. The fracture toughness is a linear function of the surface roughness of these CO ceramics.

Keywords: Clay-organic ceramics; Surface roughness; Porosity; Fracture toughness; Strength; Microstructure

1. Introduction

South Asia has a large rural population which predominantly lives at unpiped location [1]. Physical water scarcity superimposes on economic water scarcity at rural regions in South Asia [2]. Different parts of India typically showcase such a scenario [3]. Clay ceramics are accessible to this economically backward rural population [4]. Ceramics cover a wide range of applications due to their structural heterogeneity [5]. Among the different class of ceramics, clay-based ceramic filters have proven to be sustainable solutions for drinking water [6]. Several nongovernment organizations are spearheading dissemination

* Corresponding author.

of frustum-shaped clay ceramic water filter manufacture in several locations in India [7,8]. Varying the size of these clay ceramic filters and use of different filter geometries were also performed for improving the quantity of the filtrate [9,10].

Traditionally, potters provide importance to visual inspection of the fired material to judge its structural and functional quality. Therefore, the investigation should be directed to study the relationship of the dimensional parameters such as porosity and surface roughness with material toughness, load-bearing capacity, and functionality.

Ceramic water filter manufacture requires clay and plant-based waste residues as input raw materials [2]. The residues of agriculture and carpentry waste have been incorporated as raw materials [11]. The properties of clay and filler residues differ with geographical location [12,13]. The strength of ceramics is influenced by the chemical composition and porous fraction [14,15]. Relating the strength of ceramics to its surface properties and microstructure is very important for functional applications [16,17]. Modification of the material surfaces relates to changes in surface energy which affects properties of wettability and adhesion [18,19]. Furthermore, materials have distinct hydrophobic and hydrophilic properties depending on different surface roughness and capillary pore contact angles [20]. Bioreceptivity and microbial adhesion can be improved by increasing surface roughness in porous ceramics like roof tiles [21,22]. Therefore, pore features and surface roughness of materials have some correlations.

The porosities are direction-dependent parameters [21]. Liu [24] provided a polynomial expression of compressive strength as a function of porosity in hydroxyapatite-based ceramics. The increase of porosity leads to a decrease in resistance to crack propagation in clay ceramics used for filtering water [25]. It is known that pore geometry such as pore orientation angle can be used to predict Young's modulus [26]. The fracture toughness was also expressed as a power law of the pore sizes found within the clay ceramics [27–29]. Finishing or polishing process covers up flaws on ceramic surfaces effectively thus corresponds to its strength [30]. The authors reported a linear variation of failure stress with respect to the roughness of veneer ceramics [30].

The different sections below will enumerate laboratory studies on the chemical characteristics of square plate water filtration clay ceramics. Compositional correlations which affect sintering and mechanical properties were investigated [31]. The effect of porosity and surface roughness of these clay ceramics due to raw material composition was substantiated. The structural quality of the filter using simple visual surface profiling was carried out and elaborated. Discharge through square plate water filters containing 20 cm of water is modelled and compared with cylindrical and frustum-shaped filters with a water column height of 20 cm [7]. The results of the studies imply providing notion toward possible scaling of such ceramic devices [10,32]. Bimodal pore distribution in clay ceramics was found to improve its fracture resistance [33]. The directional flow of moist clay matrix during the molding process influences fracture properties of the final sintered product [33]. Failure stress of clay ceramics holds a polynomial relationship to its corresponding densities [33]. The discussion in this document will bring about the influence of fineness of the surfaces (formed during shearing

of a clay dough along with a flat boundary) of a ceramic to its fracture toughness and compressive characteristics.

2. Materials and methods

2.1. Chemical composition of raw materials

The clay samples were obtained from a clay mining area in Mokalsar, Jodhpur, Rajasthan, India. The local clay samples obtained are coarse in size. These samples are powdered manually using a wooden mallet and controlled in size using a 2 mm × 2 mm sieve (ASTM No. 10) size. The fluorescence spectroscopy-based investigation of chemical constituents (Bruker S4 Pioneer facility X-ray fluorescence (XRF)) in clay is given in Table 1. It is observed that silicates, aluminates, oxides of iron, and salts dominate the clay composition. Due to direct extraction, a large quantity of organics is also found within the local clays. Magnesium oxide content in the local clays is more than in illite and lower than in montmorillonite and metabentonite. Sodium oxide content is closer to that in illite and lower than montmorillonite [34].

2.2. Sawdust as an organic filler

The sawdust used in this work was obtained from Rajasthan Timber, Jalori Gate, Jodhpur, Rajasthan, India. This sawdust is 90% acacia wood (imported from Ghana). The sawdust is brought and sieved using 1 mm × 1 mm sieve (ASTM No. 18). The XRF spectroscopy investigation of sawdust is given in Table 2.

Table 1
Chemical composition of the clay

Chemical compounds	Weight (%)
Loss of ignition	31.026
SiO_2	43.57
Al_2O_3	11.45
Fe_2O_3	5.800
CaO	2.840
K_2O	2.02
MgO	1.710
Na_2O	0.530
P_2O_5	0.060
TiO_2	0.650

Table 2
The chemical composition of sawdust filler

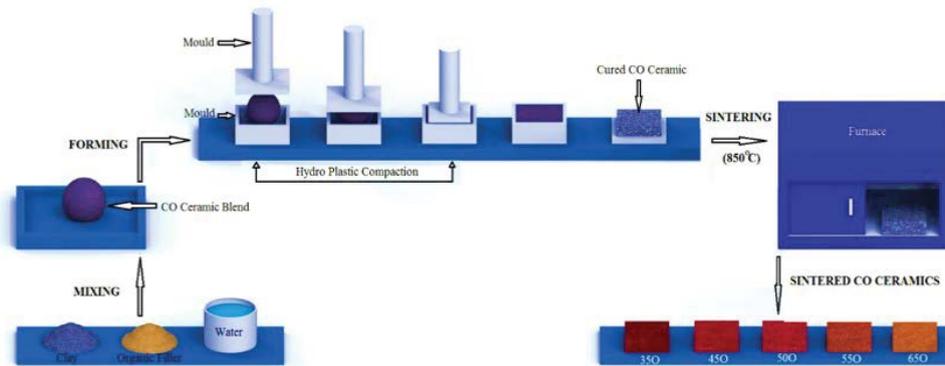| Chemical compounds	Weight (%)
Loss of ignition	91.938
SiO_2	5.77
Al_2O_3	0.160
CaO	0.990
Fe_2O_3	0.680
K_2O	0.240
MgO	0.050
P_2O_5	0.030
TiO_2	0.040

Fig. 1. Manufacturing setup for clay ceramics with the distinct organic fraction.

2.3. Forming and sintering (preparation of clay-organic ceramics)

Fig. 1. illustrates the diagrammatic representation of preparation of clay-organic ceramics. Mixtures containing local clay (C) and sawdust (O) in the volumetric ratio of (C:O) 65:35, 55:45, 50:50, 45:55, and 35:65 were prepared [33]. Precisely, 800, 840, 850, 880, and 890 mL of water was added in 1,600 mL volume of each of the respective mixtures during mixing. The mixing was performed manually (for half an hour) using hands to attain homogeneity in the composition of the individual clay-organic (CO) mix balls [35].

The moist balls are further pressed under 1.5 bar pressure to form the green composites. The dimensions of the prepared green composite samples were 15 mm in thickness and 100 mm × 100 mm in cross section. Furthermore, the samples were left for curing at room temperature until their weights stabilized. The dried samples were sintered in a programmable electric furnace [TEXCARE™ Muffle Furnace 220 V, 250 × 340 × 180 mm^3 (w×d×h)] at a temperature of 850°C [33]. The weights of the dried and sintered green composites are shown in Fig. 2. The notations of 35O, 45O, 50O, 55O, and 65O represent the composites manufactured from the 65:35, 55:45, 50:50, 45:55, and 35:65 mixtures, respectively. The percentage weight reduction of the sintered samples from the corresponding dried green composite samples were 20.1%, 30.6%, 41.6%, 42.1%, and 49.3% for the 35O, 45O, 50O, 55O, and 65O mixtures, respectively. The weights observed in 50O and 55O composites are very similar even though added water during mixing varied by 30 mL. The composites 50O and 55O showcase 45.5% reduction in ceramic weight for corresponding dried composite. The investigation into the correlations between microstructural and surface properties of the sintered samples was performed and is presented in the following sections.

2.4. Ceramic characterization

The different sintered CO ceramic samples were individually powdered using agate mortar and pestle. Powdered sample (2 mg) was mixed with 20 mg of boric acid, and the mixture is turned into a pellet using pellet presser. The pellets were analyzed in Bruker S4 Pioneer XRF instrument at the Jawaharlal Nehru University, Delhi, India, for determining the chemical composition of the samples.

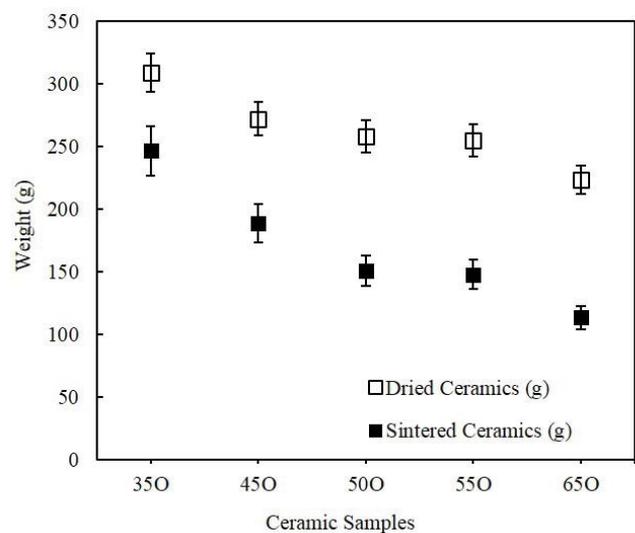The mineralogical investigation of ceramic samples was carried out in Bruker D8 advanced diffractometer using Cu–Kα

Fig. 2. Variation of weight in CO composites before and after sintering.

radiation (λ = 1.5418 Å) with a step size of 0.02 and scan speed of 0.5. Quantification of different minerals from the diffraction data was carried out using crystallographic analysis software (PANalytical X'pert High Score, PANalytical) [36].

The microstructural and densification behaviors of CO ceramics were assessed using scanning electron microscopy (SEM) (FEI, Quanta 200, MRC, MNIT Jaipur, Rajasthan, India). The ceramics were cut into 5 mm × 5 mm cross sections. Specimens were coated with palladium by low vacuum sputter coating in order to increase the conductivity of the sample to obtain superior image quality. The palladium-coated CO ceramics were placed over the specimen slots which were covered with carbon tape and locked in the chamber for imaging analysis [37].

The porosity and pore size distribution in distinct CO ceramics were determined using mercury intrusion porosimetry (MIP) (Micromeritics' AutoPore IV 9500 Series, I.I.T. Bombay, India). The MIP measurements were replicated three times. These measurements were conducted on ceramic pieces with dimensions of ~3 mm × 3 mm cross sections.

A sample set of 3 mm × 3 mm cross section was tested for mean orientation of pores using synchrotron-based

microcomputed tomography technique (BL-4 Indus 2, RRCAT Indore, India operating at 2.5 GeV, 200 mA). The micro-CT image data sets were binarized to segment the pores using a sequence of distance transformation followed by watershed segmentation method [34]. The segmented pores were uniquely labelled to determine their frequency distribution over clay matrix surface. All operations of image processing and image analysis were carried out using open source software Image [35]. Apart from the measurement of pore dimensions, the results were used to calculate permeability [7]. With the intent scaling of such materials, an example prediction of flow through square, cylindrical, and frustum shapes of filter material with the same height of 21 cm was performed. This should provide an opportunity to study scaling of distinctly shaped 5OO material filters which are used across the world by Potters for Peace [3,9,25].

2.5. Flow characterization

Following hydrodynamic models were used to predict the flow of water through the filters as illustrated in Fig. 3 [25,38–39]. Filtration was assumed to follow Darcy's flow with geometrical modifications. Filtrate production of 650–965 mL h^{-1} from the use of local frustum-shaped ceramic filter had been observed [7]. The porous ceramic media permeability k of 8.1E–14 m^2 has been utilized to model the flow [7]. The total flow through the geometries in Fig. 3 can be written as

$$Q_{\text{total}} = Q_{\text{base}} + Q_{\text{side}} \tag{1}$$

For a frustum of height h, slant height l, and a top and base radii of R_1 and R_2, respectively, the total discharge Q_{total} will be a sum of Eqs. (2) and (3).

$$Q_{\text{base}} = \frac{k}{\mu t_b} \pi R_2^2 \rho g h \tag{2}$$

$$Q_{\text{side}} = \frac{k}{\mu t_s} \int_0^h \rho g (h-z) \times 2\pi (R_1 + z\tan\theta) \frac{dz}{\cos\theta}$$

$$= \frac{\pi k \rho g h l}{3\mu t_s} \left[2R_2 + R_1\right] \tag{3}$$

Here k is the permeability of the material, μ is the dynamic viscosity of the water (8.935e-4 Pa·s) at 25°C, t_b and t_s are the thickness of the base and the sides of the geometry, respectively.

For a cylinder of height h and a radius of r, the total discharge Q_{total} will be a sum of Eqs. (4) and (5).

$$Q_{\text{base}} = \frac{k}{\mu t_b} \pi r^2 \rho g h \tag{4}$$

$$Q_{\text{side}} = \frac{k}{\mu t_s} \int_0^h \rho g (h-z) \times 2\pi r dz$$

$$= \frac{\pi r k \rho g h^2}{\mu t_s} \tag{5}$$

For a square base prism of height h and a base side s, the total discharge Q_{total} will be a sum of Eqs. (6) and (7).

$$Q_{\text{base}} = \frac{k}{\mu t_b} s^2 \rho g h \tag{6}$$

$$Q_{\text{side}} = \frac{k}{\mu t_s} \int_0^h \rho g (h-z) \times 4s dz$$

$$= \frac{2sk\rho g h^2}{\mu t_s} \tag{7}$$

2.6. Surface roughness

Samples of 35O, 45O, 50O, 55O, and 65O ceramics with 50 mm × 50 mm cross section were kept under non-contacting DektakXT® stylus surface profiler (Bruker GT-KO, IIT Kanpur, India) to analyze the surface roughness profile of the different ceramic samples. The surface roughness is evaluated at 30 distinct points over the cross section. The surface roughness measurements conformed to the methods for measuring surface texture (IS-25178-604 ISO international standard).

2.7. Mechanical characterization

The fracture toughness tests were carried out on the laboratory-based universal testing machine (Model EZ-50,
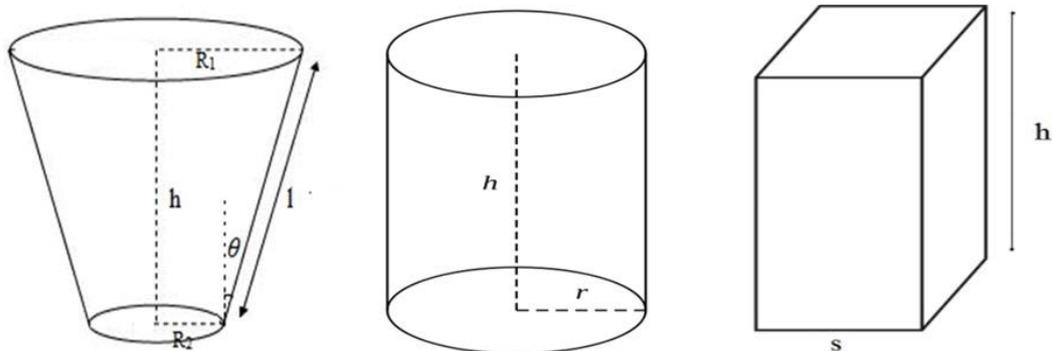

Fig. 3. The schematics of the assumed volumes of a frustum, cylinder, and square base prism.

Lloyd Instruments, Germany). The single-edge notch bend specimens were of 75 mm × 15 mm × 15 mm size. The specimens showcased a notch width of 3 mm and a depth of 0.755 mm at the centre. A loading rate of 0.1 N s^{-1} was applied during the three-point bend tests [35]. The test results corresponding to the fracture (ASTME-399-90 mode I test standard) were recorded using Nexygen material testing software (Nexygen plus 01/3366, Lloyd Instruments, Germany).

For the compressive strength test, ceramic specimens of 35 mm × 15 mm × 15 mm size were cut and extracted (Bosch GDC 120). A loading rate of 0.1 N s^{-1} was applied along the 35-mm axis until the sample was completely crushed. Load and strength data were recorded digitally using Nexygen plus material testing software. The compression tests conformed to ASTM 1358.

3. Results and discussion

3.1. X-ray fluorescence

The chemical composition of ceramics prepared from different compositional ratios is shown in Fig. 4. The sintered ceramics predominantly contained SiO_2, Al_2O_3, and Fe_2O_3. The percentage of silica, alumina, and oxides of iron decreased with an increase in the organic fraction in the fired (cured) ceramics. The presence of relatively high amounts of silica, alumina, and quartz in the 35O, 45O, and 50O samples, compared with the 55O and 65O samples (Fig. 4), will contribute to the physical properties of ceramics [40]. Higher the content of alumina in the clay, better is the refractoriness of the clay [41]. The content of alumina inversely affects the mechanical strength of ceramics [42].

The chemical composition data for clay were appended with that for the five porous clay ceramics and plotted in Fig. 5. There are 9 variable minerals listed along the abscissa of the plot in Fig. 5. This provides the 6 × 9 compositional data matrix for the six major compositions considered in this study. A multivariate analysis of the compositional data was performed (Minitab Version 16, Minitab, IIT Jodhpur Licence, India). These chemical compositions were correlated to each other, which should be manipulated to utilize these variables in the prediction of any of the major properties of these ceramics [43,44].

A new uncorrelated matrix is derived from the correlated matrix of compositional data of clay (1), 35O (2), 45O (3), 50O (4), 55O (5), and 65O (6) using principal component analysis [44]. The analysis treats the correlation matrix using a characteristic value equation to find the independent matrix of variables and eigenvalues [43]. The new independent matrix elements correspond to the principal components which express the correlation magnitude [33,43]. The eigenvalues are 5.99936, 0.00050, 0.00010, 0.00003, 0.00001, and 0.00000 (Minitab Version 16, Minitab, IIT Jodhpur Licence, India). The first component and second component are found to have corresponding high scaling factors or eigenvalues [45]. Therefore, these two components were used to explain the effects of the chemicals on each other [46].

The sign of each element defines the manner in which each of the chemical components contributes to its independent influences on the ceramic material characteristics [33]. Fig. 5 illustrates positivity in the second component due to the presence of Na_2O and K_2O. Furthermore, the negativity
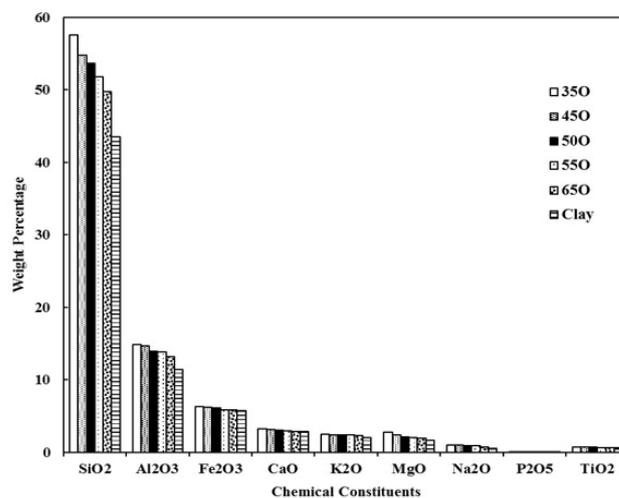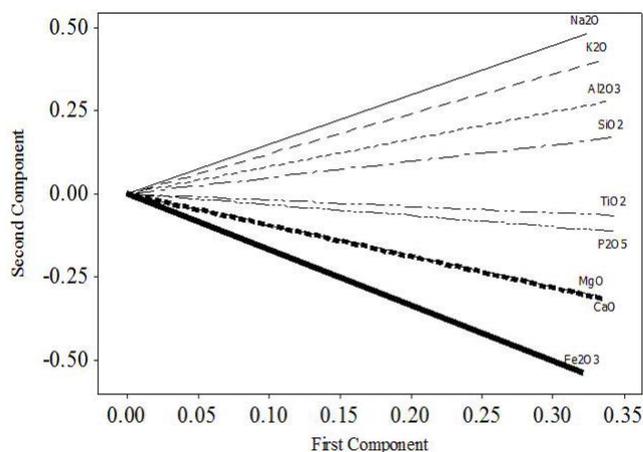
Fig. 4. Chemical composition of the CO ceramics.

Fig. 5. Loading plot showing the influence of chemicals on the microstructural properties of clay ceramics (Minitab Version 16, Minitab, IIT Jodhpur Licence).

of the second component is due to high Fe_2O_3, which is also the reason for the red color of the samples [33]. The CaO and MgO values also influence this negativity and indicate the presence of traces of carbonates such as calcites [46]. The small angles between Na_2O–K_2O and CaO–MgO compositions signify the high correlation influencing microstructural properties of these local clay ceramics [45]. This also confirms a similarity in their mode of influence [47]. Therefore, Na_2O–K_2O and CaO–MgO are said to be a prominent group or cluster which defines the presence of salinity in clays and influences its related ceramic properties. The presence of small angle between TiO_2 and P_2O_5 hints at the presence of locations of high photo-based oxidation sites for organic material and hydrophilic (attracts water, rejects oil) sites [48]. This supports bactericidal or antimicrobial characteristics of the material in the presence of light [48].

The derived two principal orthogonal components define a plane of nine different chemical compositions. The coordinates of all the chemical compositions on this plane

are projected values known as scores [49]. The score plot in Fig. 6 confirms clear distinction of properties between clusters 2–3 and 5–6. The ceramics with compositions of 2 and 3 would showcase similar properties. The 5OO (4) composition has a very distinct structural character compared with these clusters [46,50]. This hypothesis will be reflected in the further microstructural investigation. The properties of the six samples clearly lie disconnected from each other. Here, the properties of 1 (clay) and 4 (5OO) can be said to be inversely correlated since they are located at quadrants which are diagonally opposite to each other [49,50]. The closeness of 4 (5OO) to the origin of the score plot in Fig. 6 also suggests possible mirroring of sintered clay character [45].

Flow from the 5OO filter geometries of frustum, cylindrical, and square prism shapes is represented in Fig. 7. Darcy flow equations derived according to distinct geometries of prism, frustum, and cylinder and stated in Eqs. (1)–(7) have been used to illustrate the flow through ceramic filter geometries at 25°C [7].

At the fully filled condition, the square base prism provides a comparatively better discharge as compared with other geometries. An opportunity of scaling such filter is observed with varying filtrate discharge with dimensional changes. A similar coincident flow rate through the filters is observed after almost 8 h, which corresponds to flow at the head of 5 cm of water.

3.2. X-ray diffraction

The evolution of quartz, potassium feldspar, and hematite as prominent minerals within sintered ceramics can be observed from Fig. 8 [52]. The presence of high amount of silica is indicative of the occurrence of the quartz phase in ceramics. The presence of quartz influences the mechanical properties of fired ceramics [52]. The appearance of feldspar aided densification and reduced sintering time [32,54,55].

The significant changes in the intensities of quartz peaks attribute to the varying CO additive ratios. Clay ceramic water filter introduced in Rajasthan following the 5OO composition developed cracks due to thermal stress [56]. The fact being that clay artifacts do not show resistance to thermally induced stresses, and hence, a calcium carbonate addition was prescribed in this region to restrict high expansion rates of quartz [57,58].

3.3. Microstructural analysis

In all the clay, the different ceramic microstructure as shown in Fig. 9 displays the presence of the pores and interconnected tunnels through the pores.

A linear relationship between the porosity and the composition of the clay ceramics is observed from Fig. 10 [33]. The samples investigated were having pore sizes ranging between 0.003 and 360 μm.

Fig. 11 presents the large porosity contribution due to the existence of submicron range pores and pore sizes between
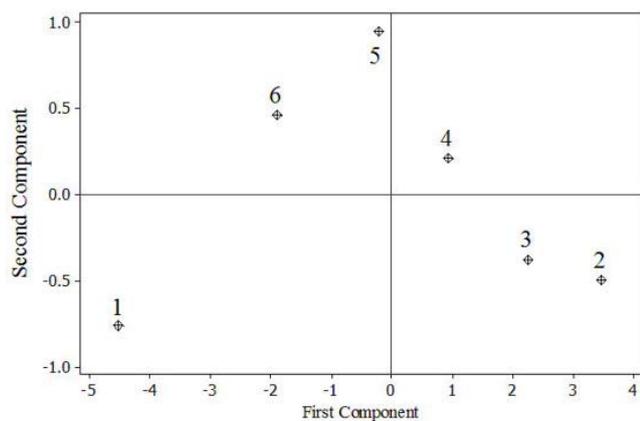
Fig. 6. The score plot of the principal components of the correlated matrix of elemental compositions of Clay (1), 35O (2), 45O (3), 50O (4), 55O (5), and 65O (6), respectively (Minitab Version 16, Minitab, IIT Jodhpur Licence).
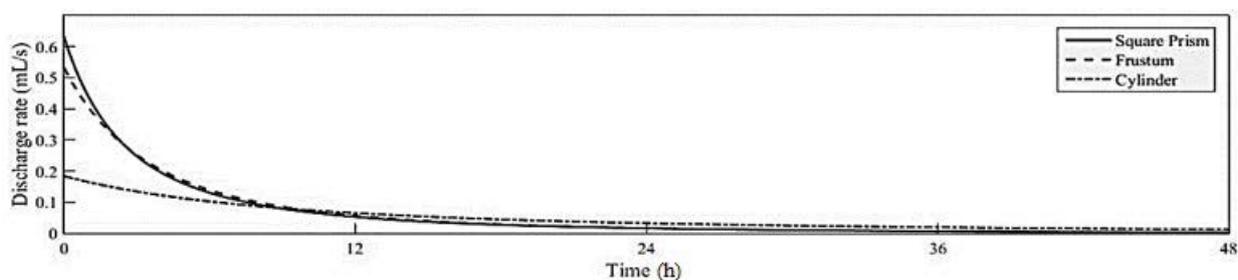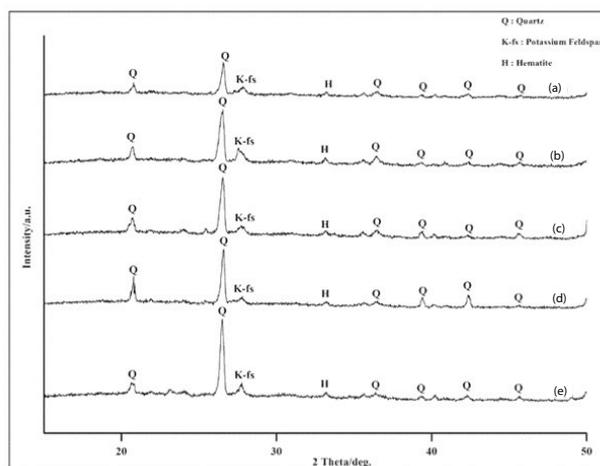
Fig. 8. X-ray diffraction pattern of fired ceramics prepared from different raw material compositional ratios (a) 65O, (b) 55O, (c) 50O, (d) 45O, and (e) 35O (Origin Pro 16, IIT Jodhpur License).

Fig. 7. Filtrate production in different 10-L capacity clay ceramic filter cured at 850°C.
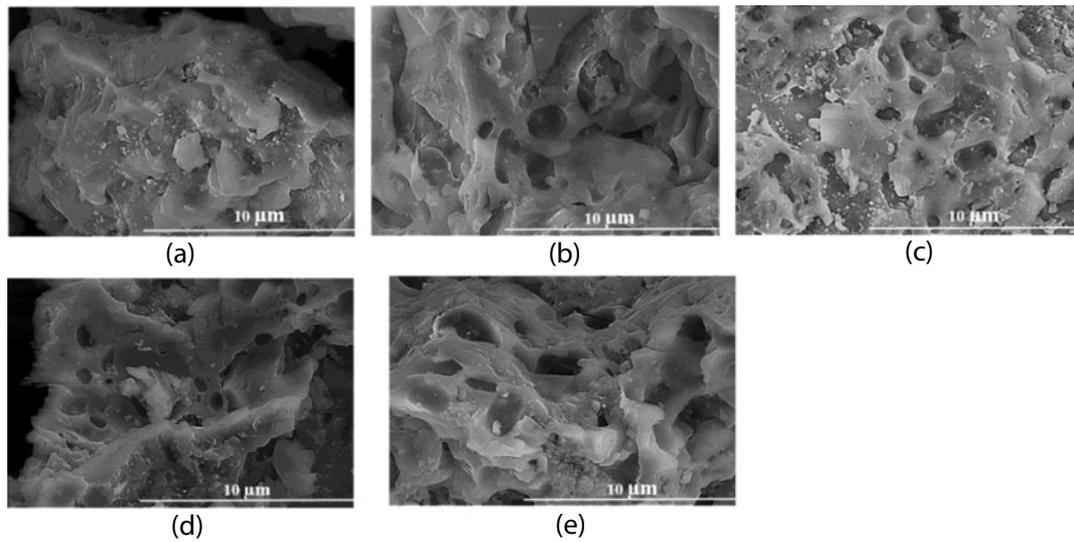
Fig. 9. Surface morphology of distinct CO ceramics at 5,000×: (a) 35O, (b) 45O, (c) 50O, (d) 55O, and (e) 65O.

Fig. 10. Porosity variation with different ceramic composition.

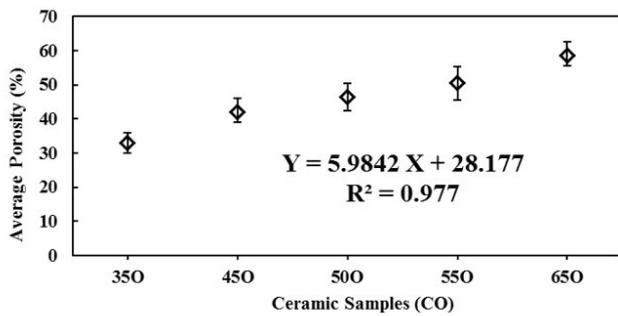

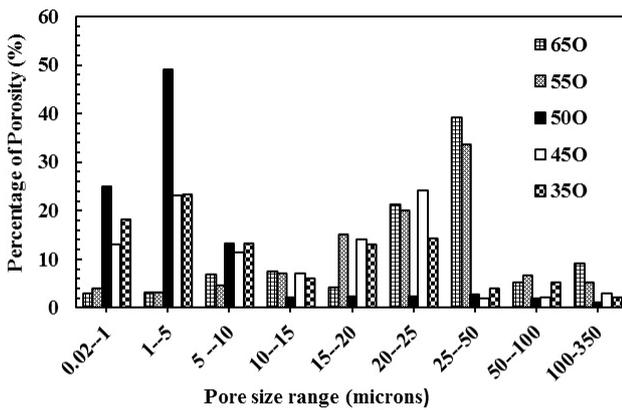Fig. 12. Pore orientation in different CO ceramics.

Fig. 11. Pore size distribution for CO ceramics with distinct organic filler content.

1 and 5 μm for 50O ceramics in comparison with other ceramic compositions. This would help to efficiently filter submicron size particles [55].

The distribution of the orientation angle shown in Fig. 12 confirms the randomness of the pores irrespective of their compositions. The area under the curves shows that there is a high density of pores orthogonal to the surface [60]. Pores perpendicular to filtration surfaces can be the best location
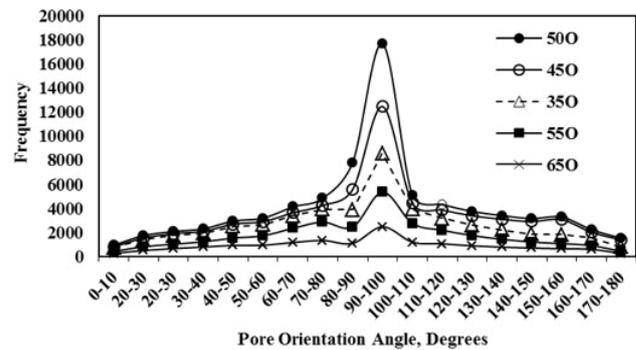
for reactions and would positively influence the filtration and percolation. The area under the orientation angle curves corresponding to angles between 85° and 105° is the maximum for 50O ceramics compared with the other ceramics analyzed through the information in Fig. 12. This information characterizes the family of CO ceramics to be good for separating the solutes from the solutions, and 50O ceramic is an efficient material that could be used in filtration [61]. Moreover, if pore orientation angles are as high as 90°, the physical properties of the porous material also get enhanced with improvement in aspect ratio [62]. The frequency, at which pores at different orientation angles are observed within a specific clay ceramic sample, will influence their overall strength [62]. Therefore, pore orientation angle data have to be utilized effectively to predict individual porous material properties.

3.4. Surface roughness

The plot of the surface roughness of the different ceramics as a function of their corresponding porosities shown in Fig. 13 appears to be a straight line. The constant term in the equation (within Fig. 14) indicated the role of intrinsic clay
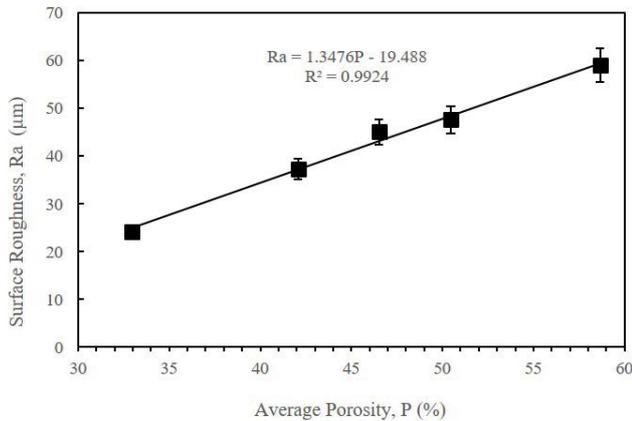
Fig. 13. Surface roughness variation with average porosity.

Fig. 14. Compressive strength as a function of surface roughness.

Fig. 15. Fracture toughness as a function of the surface roughness.

pores whose appearance is independent of the presence of the organic filler in developing the surface roughness in CO ceramics [63].

The surface flaws can influence the strength of ceramic material [64]. Surface roughness degrades mechanical properties of a material product [16]. The porosity can be a function of the material microstructure, its manufacturing process, and material property [65,66].

3.5. Compressive strength

The compressive strength displayed polynomial decrement with increasing organic filler fraction in the clay matrix as shown in Fig. 14. This linear decrement is supported by the fact that increasing the apparent porosity may result in decreasing the load-bearing capacity [32]. The cracks present in the CO ceramics extended slowly and might propagate along the compressive axis to form the crushed zone, which promoted the compressive failure [66,67]. The degree of crack resistance or propagation is associated with the occurrence of the flaws and their pore size, meaning there is a possibility that compressive strength is related with the fracture toughness [68]. This would mean that for the assessment of K_{IC}, observation should be on flaw size and their orientation which are basically pore size and their orientation angles [24,66].

The magnitude of compressive strength of different porous clay ceramics was found to be almost twice in comparison with the values of various clay-based water filters manufactured in different locations [69,35,10]. This emphasizes the geographical significance of the raw materials, process variables adopted, and thermal cycle temperature for the manufacturing of clay-based ceramics.

3.6. Fracture toughness

The average fracture toughness K_{IC} plotted against surface roughness is plotted in Fig. 15, which is fitted with a linear function. This approves the fact that a potter can visually interpret the toughness of the ceramic product. The model in Fig. 15 has a coefficient of determination of 0.9416. Earlier, the fracture toughness of the fired clay ceramics was found to vary exponentially with sintering temperature [24,70,71]. Also, the toughness of ceramics was found to be influenced
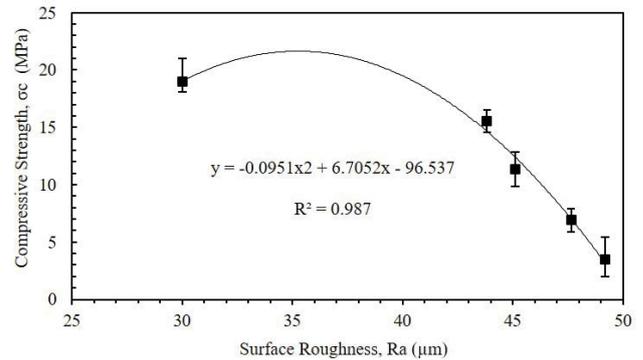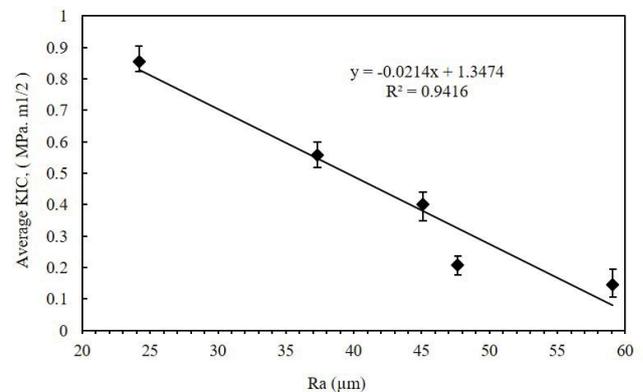
by quartz content. Improvement in quartz content ensured the toughening of the material during fracture [57].

4. Conclusion

A family of ceramic filters capable of submicron-level water contaminant removal have been characterized and studied for their physical properties. The spectroscopic analysis showed the dominance of silica, alumina, and quartz, which contributed to building the strength of the fired ceramics. The presence of iron oxide was responsible for the reddish color in the fired ceramics. The existence of high amounts flux materials such as K_2O and Na_2O along with Fe_2O_3 has contributed to significant densification of CO ceramics (up to 50% organic fraction). The presence of Na_2O, K_2O, CaO, and MgO hints at the possible saline nature of the clay. Pores tend to be orthogonal irrespective of the volume fraction of raw materials which is representative of efficient filtration characteristics. Sample with 50% organic fraction was characterized by a large number of submicron pores and a large density of orthogonally orientated pores. The degree of the surface roughness increased in proportion with the pore fraction. The compressive strength displayed linearly decreasing trend with the increased surface roughness of CO ceramics. The fracture toughness of CO ceramics showed polynomial decrement with the increasing surface roughness. A novel multiparameter model to establish the

empirical relationship between the fracture toughness of CO ceramics, pore orientation angle, and a new material factor is proposed. The implications of the results will assist in the optimization of structural properties by studying the surface parameters of similar CO ceramics with application in the area of drinking water filtration. Scaling of such filters can be a viable way to increase filtrate production.

Acknowledgement

References

[1]   H.P. Rosegrant, M.W. Binswanger, Markets in tradable water rights: potential for efficiency gains in developing country water resource allocation, World Dev., 22 (1994) 1613–1625.

[2]   A.K. Plappally, J.H. Lienhard, Costs for water supply, treatment, end-use and reclamation, Desal. Wat. Treat., 51 (2013) 200–232.

[3]   A. Plappally, A. Hasija, J. Kusins, M. Jhaver, A. Chee, Water use and related costs at households in western and northern parts of India, Hydrol. Curr. Res., 4 (2013) 2.

[4]   B. Saraswati, Pottery-Making Cultures and Indian Civilization, Abhinav Publications, Newdelhi, India, 1978.

[5]   W.M. Carty, P.W. Lednor, Monolithic ceramics and heterogeneous catalysts: honeycombs and foams, Curr. Opin. Solid State Mater. Sci., 1 (1996) 88–95.

[6]   M.D. Sobsey, C.E. Stauber, L.M. Casanova, J.M. Brown, M.A. Elliott, Point of use household drinking water filtration: a practical, effective solution for providing sustained access to safe drinking water in the developing world, Environ. Sci. Technol., 42 (2008) 4261–4267.

[7]   S. Gupta, A. Kaurwar, R.K. Satankar, K. Usha, A.K. Plappally, Flow, filtration and petro physical properties of ceramic plate ware gravity water filter and its variation with long term cyclic water loading, In Proceedings of from Pollution to Purification (International Conference on Water 2016), Organized by IUIC, ASCEED & School of Environmental Sciences, Mahatma Gandhi University, Kottayam, 2016.

[8]   Available from http://www2.ichcap.org/publications-archive/contribution-of-intangible-cultural-heritage-to-sustainable-development-in-south-asia/.

[9]   S. Murcott, Implementation, critical factors and challenges to scale-up of household drinking water treatment and safe storage systems, Cambridge, Massachusetts Institute of Technology, MA, 2006.

[10] E. Annan, K. Kan-Dapaah, S.T. Azeko, K. Mustapha, J. Asare, M.G.Z. Kana, W. Soboyejo, Clay mixtures and the mechanical properties of microporous and nanoporous ceramic water filters, J. Mater. Civ. Eng., 28 (2016) 04016105.

[11] V.C.S. Prasad, V. Ganvir, DMAIC Approach in Rural Technology—An Application to Making of Water Filters, Trans. Indian Ceram. Soc., 65 (2006) 215–221.

[12] R.M. Lark, R. Webster, Changes in variance and correlation of soil properties with scale and location: analysis using an adapted maximal overlap discrete wavelet transform, Eur. J. Soil Sci., 52 (2001) 547–562.

[13] F. Higashikawa, C. Silva, B. Wagner, Chemical and physical properties of organic residues, Rev. Bras. Cienc. Solo, 34 (2010) 1742–1752.

[14] G. Cultrone, E. Sebastián, K. Elert, M.J. De la Torre, C. Rodriguez–Navarro, Influence of mineralogy and firing temperature on the porosity of bricks, J. Eur. Ceram. Soc., 24 (2004) 547–564.

[15] F.F. Lange, Powder processing science and technology for increased reliability, J. Am. Ceram. Soc., 72 (1989) 3–15.

[16] J. Tay, Bricks manufactured from sludge, J. Environ. Eng., 113 (1987) 278–284.

[17] U. Lohbauer, F.A. Müller, A. Petschelt, Influence of surface roughness on mechanical strength of resin composite versus glass ceramic materials, Dent. Mater., 24 (2008) 250–256.

[18] J. Lawrence, L. Li, J.T. Spencer, Diode laser modification of ceramic material surface properties for improved wettability and adhesion, Appl. Surf. Sci., 138 (1999) 388–393.

[19] R. Shuttleworth, G.L.J. Bailey, The spreading of a liquid over a rough solid, Faraday Soc., 3 (1948) 16–22.

[20] A. Gajewski, Contact angle and sessile drop diameter hysteresis on metal surfaces, Int. J. Heat Mass Transfer, 51 (2008) 4628–4636.

[21] M.F. Gazulla, E. Sánchez, J.M. González, M.C. Portillo, M. Orduña, Relationship between certain ceramic roofing tile characteristics and biodeterioration, J. Eur. Ceram. Soc., 31 (2011) 2753–2761.

[22] H. Rashid, The effect of surface roughness on ceramics used in dentistry: a review of literature, Eur. J. Dent., 8 (2014) 571.

[23] A. Narasimhan, Essentials of Heat and Fluid Flow in Porous Media, CRC Press, NY, 2013.

[24] D.M. Liu, Influence of porosity and pore size on the compressive strength of porous hydroxyapatite ceramic, Ceram. Int., 23 (1997) 135–139.

[25] I. Yakub, J. Du, W.O. Soboyejo, Mechanical properties, modeling and design of porous clay ceramics, Mater. Sci. Eng., A., 558 (2012) 21–29.

[26] A.R. Boccaccini, Influence of stress concentrations on the mechanical property–porosity correlation in porous materials, J. Mater. Sci. Lett., 17 (1998) 1273–1275.

[27] S.K. Maiti, M.F. Ashby, L.J. Gibson, Fracture toughness of brittle cellular solids, Scr. Metall., 18 (1984) 213–217.

[28] P. Sin, R. Veinthal, F. Sergejev, M. Antonov, I. Stubna, Fracture toughness of ceramics fired at different temperatures, Mater. Sci., 18 (2012) 90–92.

[29] M. D'Orazio, G. Cursio, L. Graziani, L. Aquilanti, A. Osimani, F. Clementi, C. Yéprémian, V. Lariccia, S. Amoroso, Effects of water absorption and surface roughness on the bioreceptivity of ETICS compared to clay bricks, Build. Environ., 77 (2014) 20–28.

[30] H. Fischer, M. Schäfer, R. Marx, Effect of surface roughness on flexural strength of veneer ceramics, J. Dent. Res., 82 (2003) 972–975.

[31] C. Kramer, Ceramic ethnoarchaeology, Annu. Rev. Anthropol., 14 (1985) 77–102.

[32] A. Kaurwar, R. Satankar, S. Gupta, U. Aravind, K. Kothari, A. Soboyejo, A.K. Plappally, Functional demarcation of traditional off-white colored water pots manufactured from Rajasthan clayey soils and red colored water pots from Gujarat clayey soils using spectrographic, cooling and strength studies–a case study from Jodhpur, Rajasthan, India, MRS Adv., 2 (2017) 2027–2032.

[33] A.K. Plappally, I. Yakub, L.C. Brown, W.O. Soboyejo, A.B.O. Soboyejo, Physical properties of porous clay ceramic-ware, J. Eng. Mater. Technol., 133 (2011) 031004.

[34] D. Carroll, H.C. Starkey, Reactivity of clay minerals with acids and alkalies, Clays Clay Miner., 19 (1971) 321–333.

[35] A. Plappally, Theoretical and empirical modeling of flow, strength, leaching and micro-structural characteristics of V shaped porous ceramic water filters, Ph.D Thesis, Ohio State University, 2010.

[36] T. Degen, M. Sadki, E. Bron, U. König, G. Nénert, The highscore suite, Powder Diffr., 29 (2014) S13–S18.

[37] K.R. Lyman, C.E. Newbury, D.E. Goldstein, J. Williams, D.B. Romig Jr., A.D. Armstrong, J. Peters, Scanning Electron Microscopy, X-Ray Microanalysis and Analytical Electron Microscopy: A Laboratory Workbook, Springer, US, 2012.

[38] D. Van Halem, Ceramic silver impregnated pot filters for household drinking water treatment in developing countries,

Department of Water Management, Faculty of Civil Engineering, Delft University of Technology, Netherlands, 2006.

[39] C. Carlson, S.M. Hussain, A.M. Schrand, L. Braydich-Stolle, K.L. Hess, R.L. Jones, J.J. Schlager, Unique cellular interaction of silver nanoparticles: size-dependent generation of reactive oxygen species, J. Phys. Chem., 11 (2008) 13608–13619.

[40] F.A.C. Milheiro, M.N. Freire, A.G.P. Silva, J.N.F. Holanda, Densification behaviour of a red firing Brazilian kaolinitic clay, Ceram. Int., 31 (2005) 757–763.

[41] H. Katsuki, J. Kim, S.J. Kim, S.J. Kim, J.H. Pee, W.S. Cho, Influence of alumina content in the raw clay on the sintering behavior of Karatsu ware, J. Ceram. Soc. Jpn., 124 (8) 833–837.

[42] H. Mesrar, A. Sadiki, A. Faleh, L. Quijano, L. Gaspar, A. Navas, Vertical and lateral distribution of fallout 137Cs and soil properties along representative toposequences of central Rif, Morocco, J. Environ. Radioact., 169 (2017) 27–39.

[43] A.B.O. Soboyejo, H.E. Ozkan, J.C. Papritan, W.O. Soboyejo, A new multiparameter approach to the prediction of wear rates in agricultural sprayer nozzles, J. Test. Eval., 29 (2001) 372–379.

[44] C.T. Haan, Statistical Methods in Hydrology, The Iowa State University Press, Ames, Iowa, 1994, p. 378.

[45] J. Guigue, O. Mathieu, S. Mounier, Y. Lucas, R. Laffont, P. Amiotte-Suchet, J. Lévêque, The use of 3D-Fluorescence and potential biodegradability for the comparison of extraction procedures of water-extractable organic matter in soils, Presentation at WOMS13 workshop on organic matter spectroscopy - IHSS Day at Toulon, France, 2013

[46] R.R. Pullanagari, I.J. Yule, M.P. Tuohy, M.J. Hedley, R.A. Dynes, W.M. King, In-field hyperspectral proximal sensing for estimating quality parameters of mixed pasture, Precis. Agric., 13 (2012) 351–369.

[47] C. Papachristodoulou, A. Oikonomou, K. Ioannides, K. Gravani, A study of ancient pottery by means of X-ray fluorescence spectroscopy, multivariate statistics and mineralogical analysis, Anal. Chim. Acta, 573 (2006) 347–353.

[48] J. Fu, Photocatalytic properties of TiO_2–P_2O_5 glass ceramics, Mater. Res. Bull., 46 (2011) 2523–2526.

[49] L. Eriksson, T. Byrne, E. Johansson, J. Trygg, C. Vikström, Multi- and Megavariate Data Analysis Basic Principles and Application, Umetrics Academy, Sweden, 2013, p. 1.

[50] R. Satankar, A. Kaurwar, S. Gupta, K. Usha, S.T. Azeko, W.O. Soboyejo, A.B.O. Soboyejo, Role of equine ordure in enhancing physical and mechanical properties of natural bio-active composites, Apple Academic Press, NY, 2018.

[51] R.K. Satankar, A. Kaurwar, S. Gupta, A. Plappally, Horse dung and soil based composites for construction of aesthetic shelves in rural homes of western Rajasthan, J. Environ. Nanotechnol., 6 (2017) 43–47.

[52] C. Manoharan, P. Sutharsan, S. Dhanapandian, Venkatachalapathy, Characteristics of some clay materials from Tamilnadu, India, and their possible ceramic uses, Cerâmica, 58 (2012) 412–418.

[53] L. Schultz, Quantitative interpretation of mineralogical composition from X-ray and chemical data for the Pierre Shale (No. 391-C), 1964.

[54] V. Kilikoglou, G. Vekinis, Y. Maniatis, P.M. Day, Mechanical performance of quartz-tempered ceramics: part I, strength and toughness, Archaeometry, 40 (1998) 261–279.

[55] J.F. Wu, H. Cheng, X.H. Xu, T.F. Deng, Effect of sintering aids on the densification of andalusite ceramics, Adv. Mater. Res., 842 (2014) 78–82.

[56] S. Gupta, R. Satankar, A. Kaurwar, U. Aravind, M. Sharif, A. Plappally, Household production of ceramic water filters in Western Rajasthan, India, Int. J. Serv. Learn. Eng., 13 (2018) 53–66.

[57] S. Buys, V. Oakley, Conservation and Restoration of Ceramics, Routledge, Taylor & Francis Ltd, United Kingdom, 2014.

[58] A. Kaurwar, S. Gupta, R. Satankar, A. Plappally, Marble slurry as a potential ceramic water filtration material: comparative analysis with machined Fe powder and clay ceramics for effectiveness in As removal from water at point of use, Poster Presented at 3rd International Conference on Desalination Using Membrane Technology, Spain, April, 2017.

[59] M. Youmoue, R.T. Fongang, J.C. Sofack, E. Kamseu, U.C. Melo, I.K. Tonle, C. Leonelli, S. Rossignol, Design of ceramic filters using Clay/Sawdust composites: effect of pore network on the hydraulic permeability, Ceram. Int., 43 (2017) 4496–4507.

[60] C. Robertson, R. Beanland, S.A. Boden, A.L. Hector, R.J. Kashtiban, J. Sloan, D.C. Smith, A. Walcarius, Ordered mesoporous silica films with pores oriented perpendicular to a titanium nitride substrate, Phys. Chem. Chem. Phys., 17 (2015) 4763–4770.

[61] M. Wooten, Nanofiltration membranes from oriented mesoporous silica thin films, University of Kentucky, 2014, ACS Appl. Mater. Interfaces, (2016) 21806–21815.

[62] L. Griffiths, M.J. Heap, T. Xu, C.F. Chen, P.J. Baud, The influence of pore geometry and orientation on the strength and stiffness of porous rock, J. Struct. Geol., 96 (2017) 149–160.

[63] A.T. Servi, An experimental and analytical exploration of the effects of manufacturing parameters on ceramic pot filter performance, Massachusetts Institute of Technology, Cambridge, Massachusetts, 2013.

[64] W. Teughels, N. Van Assche, I. Sliepen, M. Quirynen, Effect of material characteristics and/or surface topography on biofilm development, Clin. Oral Implants Res.,17 (2006) 68–81.

[65] Y. Shao, B. Li, S.Y. Liang, Predictive modeling of surface roughness in grinding of ceramics, Mach. Sci. Technol., 19 (2015) 325–338.

[66] D. Jones, M. Ashby, Engineering Materials 2: An Introduction to Microstructures, Processing and Design, Butterworth-Heinemann, 2005.

[67] R.W. Davidge, A.G. Evans, The strength of ceramics, Mater. Sci. Eng., 6 (1970) 281–298.

[68] W. Soboyejo, Mechanical Properties of Engineered Materials, CRC Press, New York, 2002.

[69] I. Yakub, Micro- and Nano-porous Adsorptive Materials for Removal of Contaminants from Water at Point-of-use, Ph.D Thesis, Princeton University, Princeton, New Jersey, 2012.

[70] V.G. Lee, T.H. Yeh, Sintering effects on the development of mechanical properties of fired clay ceramics, Mater. Sci. Eng., 485 (2008) 5–13.

[71] S. Freiman, Fracture Mechanics for Ceramics, Rocks, and Concrete: A Symposium, J. ASTM Int., 745 (1981) 237–256.